Magnetic sponge like behavior in a heterobimetallic cyanide bridged 1D ladder chain

Mayurika Das,[†] Sujit Kamilya,[†] Sakshi Mehta,[†] Radovan Herchel[,§] and Abhishake Mondal*[,†]*

[†]*Solid State and Structural Chemistry Unit, Indian Institute of Science, Sir C V Raman Road, Bangalore 560012, India.*

[§]*Department of Inorganic Chemistry, Faculty of Science, Palacky University, 17. listopadu 12, CZ-771 46 Olomouc, Czech Republic.*

ABSTRACT

A two-dimensional coordination complex {[Mn(Me-im)$_3$(H_2O)][Cr(CN)$_6$]0.5[Mn(EtOH)$_2$]}(**1**) (Me-im= 1-Methylimidazole) has been synthesized by following the "building-block" strategy from the reaction between $[Cr(CN)_6]^{3-}$ and Mn(II) with monodentate 1-methylimidazole ligand. The complex was characterized by single-crystal X-ray diffraction analyses, magnetic, gas adsorption and spectroscopic studies. Crystal structure analyses reveal that in the 2D network is formed, the central Cr is linked to two Mn centers of different coordination environments in the [$CrMn_2$] asymmetric unit by Cr^{III}-CN-Mn^{II} bridges. Extension of the 2D network forms "1D ladder like chains" of finite width. N_2 gas adsorption studies on desolvated sample reveals a Type II adsorption isotherm at 77 K. Magnetic studies of 1 reveal strong ferrimagnetic ordering with T_C= 2.15 K. In an attempt to increase the ordering temperature, the magnetic sponge property has also been investigated for this system by successive desolvation and resolvation, and likewise an increase in the ordering temperature has been observed.

INTRODUCTION

In the past decade, molecular magnetism has emerged as an important means to understand the fundamental aspects of magnetic interactions and magneto-structural correlations.[1] Molecular magnets have shown potential application in quantum computing[2], data storage and molecule-based spintronics devices.[3] In this respect, single molecule magnets (SMMs)[4] and single chain magnets (SCMs)[5] have gained tremendous importance because the slow relaxation of magnetization depends heavily on the magnetic interactions along the chain (for SCMs), high-spin ground state (S_T) and strong uniaxial magnetic anisotropy (D).[6] However, the assembly of magnetic building blocks to form higher dimensional molecular systems can also be used to obtain classical magnets[7, 8] where high critical temperatures can be obtained. To generate such "high T_C" molecular magnetic systems, a suitable "*solvatomagnetism*" effect is generally observed where loss of the solvent molecules renders improvement in the structural ordering and in extension, the magnetic ordering of such systems. Such molecules, where removal/incorporation of specific coordinated/uncoordinated solvent molecules influences the magnetic behaviour are termed "molecular magnetic sponges" which was first used by Prof. Olivier Kahn in 1999[9].

One of the ways to rationally synthesize heterometallic systems having the magnetic sponge property is to adopt the "building block" strategy[10] where precursors can be used to control the dimensionality of the final complex.[11] Cyanide-based precursors provide tremendous opportunities here as the cyanide ligand facilitates strong magnetic interactions *via* bridging metal centres.[12] Likewise, in recent literature, there have been some reports of cyanide bridged magnetic sponge systems using hexacyanometallate and octacyanometallate building blocks which show considerable improvement in the magnetic ordering temperatures, upon desolvation[13]. High-spin hexacyanometallates of the formula $[M(CN)_6]^{3-}$ (M=Fe, Cr) have been used in the past because of their paramagnetic ground state.[14] For example, in $[Cr(CN)_6]^{3-}$, Cr(III) has three unpaired electrons (t_{2g}^3 (O_h)) to function as a cyanide-donor ligand to form heterometallic higher-dimensional molecular systems that show high T_C molecular magnetism property with long range magnetic ordering.[15] On the other side, Mn(II) (t_{2g}^3 e_g^2 (O_h)) in high-spin state having five unpaired electrons enables

the strong ferromagnetic interactions at high and low temperatures through the Cr^{III}-CN-Mn^{II} bridges.[16] In this regard, the PBA of CrMn with the molecular formula $V^{II}[Cr^{III}(CN)_6]_{0.86}.2.8H_2O$[7] reported by Verdauger *et al* shows a remarkable T_C of 315 K, hence molecular systems based on CrMn are also expected to show T_C at high temperatures. Herein, we report for the first time, a heterometallic cyanide-bridged two-dimensional [$CrMn_2$] coordination network using monodentate ligand, that shows strong ferromagnetic interactions and long-range magnetic ordering at low temperatures.

In this work, using "building block approach" we have synthesized the 2D coordination network, {[$Mn(Me\text{-}im)_3(H_2O)$][$Cr(CN)_6$]0.5[$Mn(EtOH)_2$]}(**1**), the desolvated form (**1.des**) and the resolvated form (**1.res**) and explored the structural, adsorption, magnetic and spectroscopic properties (Me-im= 1-Methylimidazole).

RESULTS AND DISCUSSION

Synthesis and characterization. The reaction of $[NBu_4]_3[Cr(CN)_6]$ with $Mn(ClO_4)_2.6H_2O$ and 1-Methylimidazole in CH_3CN/EtOH (1:1) resulted in a colourless solution that on slow evaporation yielded colourless long rectangular crystals in good yield (~32 %). The purity of **1** was confirmed by elemental analyses and PXRD measurements (**Figure S1**). The TGA analysis of **1** (**Figure S2**) shows that it undergoes a 7.4 % weight loss till 342 K, due to partial loss of bonded solvent molecules (more accurately 1 molecule of bonded ethanol), after which it is stable up to 460 K after which it steadily loses weight till 573 K. The probable reason for the slight deviation in the experimental PXRD pattern is due to the different measurement temperatures (room temperature (298 K) and simulated (120 K)).

Scheme 1. Schematic Presentation of Synthesis of Complex **1**.

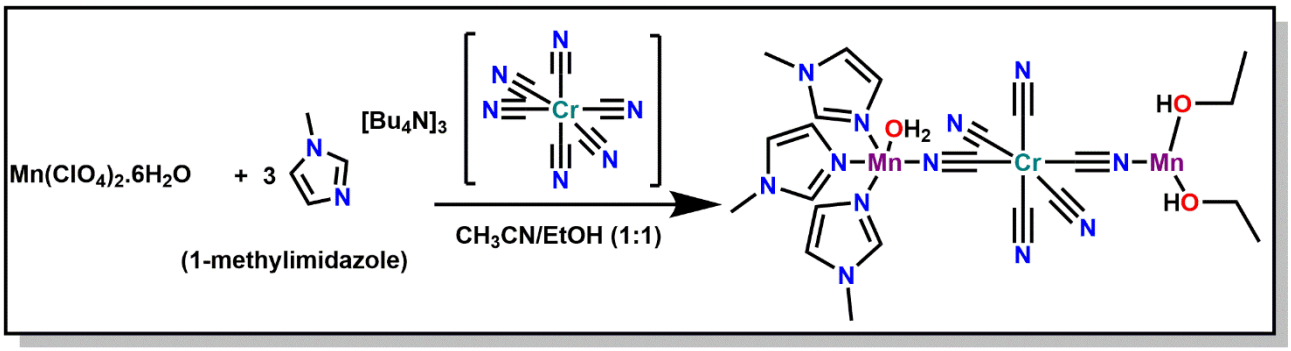

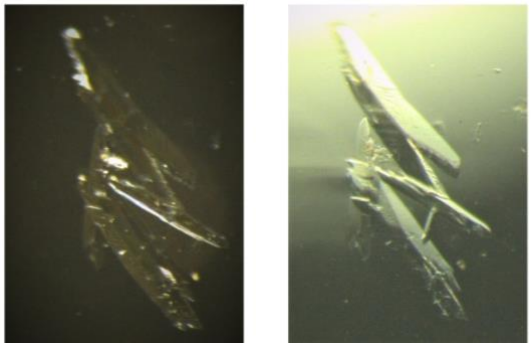

Figure 1. Image of crystals of complex **1**

Crystal Structures Analyses. Single crystal X-ray structure analyses were carried out on a suitable single crystal of **1** at 120 K (**Table 1-3, ESI**) where **1** crystallizes in monoclinic space group $P\,2_1/n$ (Z=2). The asymmetric unit (**Figure 2**) contains a $[CrMn_{1.5}]$ unit where the $[Cr(CN)_6]^{3-}$ unit that is bridged to two Mn centres by the cyanide ligand and adopts an octahedral geometry (continuous shape measures (CShM) program [17], **Table 4, ESI**) with CrC_6 surrounding from four bridging and two terminal cyanide ligands. One of the Mn centres, Mn1 with MnN_4O_2 coordination surrounding in which Mn1 is coordinated to four nitrogen donor atoms from the bridging cyanide ligands and two oxygen donor atoms from ethanol molecules, adopts an octahedral geometry (**Table 4**). This Mn centre lies in a special position and is shared simultaneously by the two Cr centres in the molecular unit (*i.e.*, two asymmetric units). The other Mn centre, Mn2 also adopts octahedral geometry (**Table 4**) with N_5O coordination surrounding in which Mn2 is coordinated to three nitrogen donor atoms from 1-methylimidazole, two nitrogen donor atoms from the bridging cyanide ligands and one oxygen donor atom from water molecule. The octahedral distortion

parameters for Cr1, Mn1 and Mn2 centres have also been calculated using the Octadist program[18] and have been listed in **Table 5, ESI**.

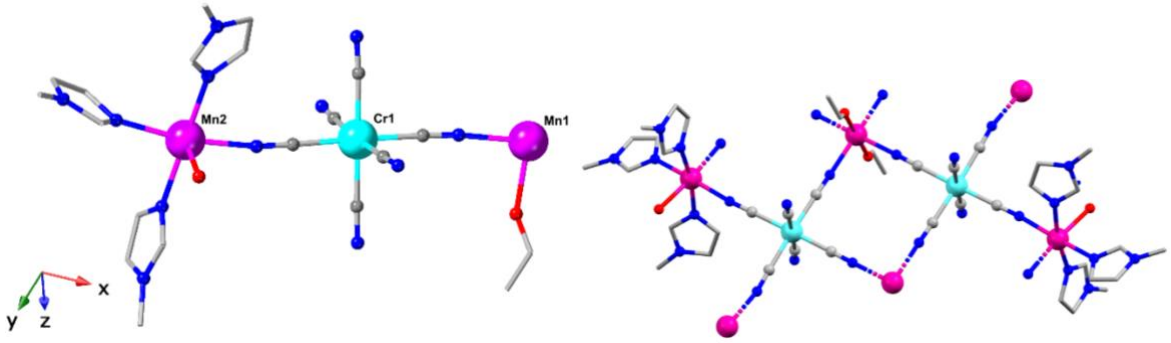

Figure 2. Perspective view of asymmetric unit (left) and molecular unit (right) of **1**. Hydrogen atoms are omitted for clarity. (Mn: magenta, Cr: cyan, C: black, grey, N: blue, O: red.)

The $[CrMn_{1.5}]$ unit when expanded in various directions forms an infinite 1D chain with alternate Cr and Mn atoms (**Figure 3, Figure S3**). At 120 K, the Cr-C bond distances in **1** lie in the range of 2.050(5)-2.079(5) Å, corresponding to Cr(III) state in octahedral geometry.[19] The average Mn2-N bond distance is 2.244 Å which corresponds to a Mn(II) in HS state. The Mn1-N distance from bridging cyanide is 2.212 Å that indicates that Mn1 is also present in the Mn(II) state. From the bond angles, the C-Cr-C(cis) angles are close to 90 ° while the C-Cr-C(trans) bond angles are close to 180 °. The Cr-C-N angles show a slight deviation from linearity [175.5(5)- 178.5(5) °] which is expected from literature values.[20] The distance between two diagonally opposite Cr atoms and Mn atoms is 7.689 Å which is the pore size of the tetragonal void in the 1D network (**Figure 3**).

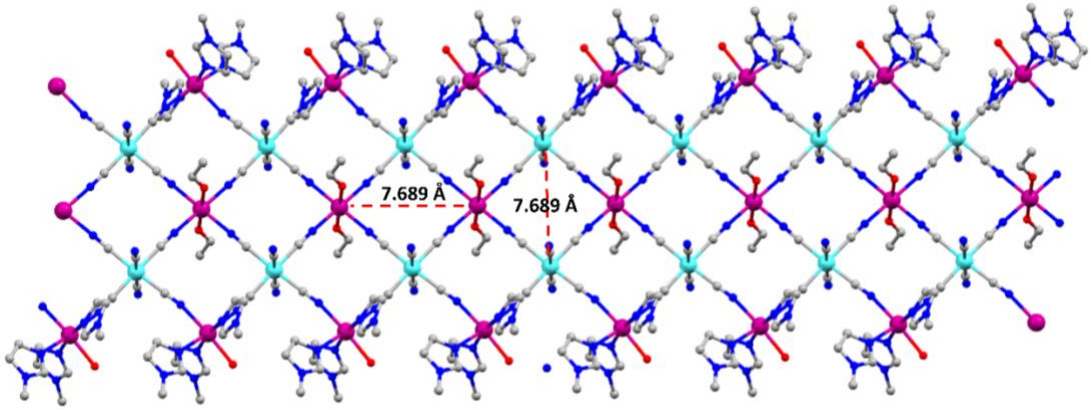

Figure 3: View along c direction in **1**. Hydrogen atoms are omitted for clarity. (Mn: magenta, Cr: cyan, C: black, grey, N: blue, O: red.)

Careful analyses of the structure revealed that the infinite 1D chain resembles a ribbon of finite width, *i.e.*, the plane formed on expanding the short contacts is of infinite length only along a-axis, along other axes the network cannot be extended beyond Mn2-Cr1-Mn1-Cr1-Mn2 unit. This finite Mn2-Cr1-Mn1-Cr1-Mn2 unit forming infinite one-dimensional chains along a-axis are somewhat stacked one above the other giving the impression of "1D ladder like chains" (**Figure 4**). These "ladder like chains" are however, not interconnected, they are weakly held together by CH-π interactions.

Several intermolecular H-bonding interactions were also observed between the terminal cyanide N and solvent molecules (water, ethanol) that are shown in **Figure S5**.

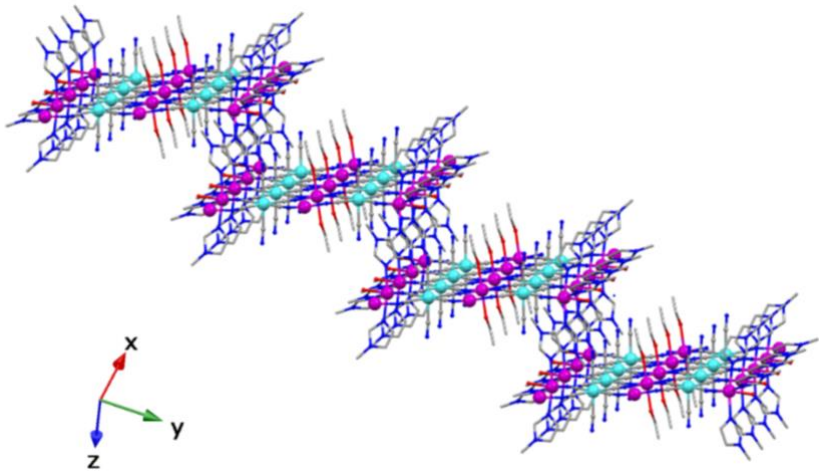

Figure 4. A view of the 1D ladder-like chains formed on extension of short contacts in **1**. (Mn: magenta, Cr: cyan, C: black, grey, N: blue, O: red.)

A number of attempts were made to obtain the crystal structure of the desolvated and resolvated phases (**1.des** and **1.res**) but no fruitful results could be obtained due to the poor crystal quality.

Spectroscopic studies. UV-Vis/NIR spectroscopy is used to give an insight into the electronic states of the metal centres. The solid-state spectrum of **1** (**Figure S5**) displays a strong absorption band at 265 nm which is ascribed to the π–π* transition coming from the methylimidazole moiety. A relatively weaker band is present at around 303 nm which can be assigned to the metal-to-ligand charge-transfer band coming from Mn^{II} → Methylimidazole ligand.[21] There is another broad band centered at around 369 nm which is due to the electronic transitions coming from the Cr^{III} centre ($^4T_{2g} \leftarrow {}^4A_{2g}$)[22]. The UV spectrum of **1.des** also follows a similar trend.

It is well known that IR spectroscopy is an important tool to characterize the electronic state and bridging mode of cyanide-bridged metal complexes since the cyanide stretching frequency (ν_{CN}) is quite sensitive to the oxidation state and spin state of the bridged metal centre. IR measurements carried out on **1** (**Figure S6**) show the characteristic ν_{CN} stretches at 2145 and 2130 cm^{-1}, that is quite shifted from the building block $[NBu_4]_3[Cr(CN)_6]$ where the ν_{CN} stretch is seen at 2110 cm^{-1}. These correspond to the bridged cyanide (*i.e.,* Cr^{III}_{LS}-CN-Mn^{II}_{HS}) and terminal cyanide stretches, respectively.[23] The IR spectrum also shows the characteristic $\nu_{=C-H}$ and $\nu_{C=N}$ stretches at 3135 and 1625 cm^{-1} respectively coming from the 1-methylimidazole ligand. In **1.des**, the ν_{CN} of {Cr^{II}-CN-Mn^{II}} unit is blue shifted to 2151 cm^{-1} while the terminal cyanide stretch shifts to 2123 cm^{-1}. Also, the ν_{O-H} stretch at 3300 cm^{-1} vanishes which indicates the complete removal of ethanol molecules. Again in **1.res**, the ν_{CN} of {Cr^{II}-CN-Mn^{II}} unit comes back to 2150 cm^{-1} and the terminal cyanide shifts to 2133 cm^{-1}.

Variable-temperature IR studies were performed on **1** in the temperature range of 300- 120 K (**Figure S7, Figure S8**) and 300- 400 K (**Figure S9, Figure S10**) in both cooling and heating modes. While decreasing the temperature to 120 K, the ν_{CN} (bridging) stretch shows a small shift of 2150-2155 cm^{-1}

(**Figure S8**) which is reversible during the heating cycle, while the terminal cyanide stretch remains almost unchanged with change in temperature.

Gas adsorption studies. N_2 adsorption studies were performed on the desolvated sample **1.des** at 77 K to understand the nature of porosity of the sample. It was seen that **1.des** follows a Type II adsorption isotherm (**Figure S11**) indicating that the sample is mesoporous (with a mean pore diameter of 102.76 nm and average surface area of 3.3679 m^2g^{-1} (BET Plot)), therefore, mainly surface adsorption takes place.

Magnetic studies. Magnetic measurements were performed on **1** in the temperature range of 1.9-300 K under an applied DC field of 1000 and 10000 Oe to determine the thermal dependence of the χT (χ is the is magnetic susceptibility equal to *M/H* per [$CrMn_{1.5}$] unit) as a function of temperature (**Figure 5, left**). At 300 K, the measured χT value is 5.89 $cm^3mol^{-1}K$, which is lower than the spin-only χT value of 8.437 $cm^3mol^{-1}K$ (g= 2.0) that is expected for one [$CrMn_{1.5}$] unit with Cr(III) ion having $t_{2g}^3e_g^0$ electronic configuration with *S*=3/2 and Mn(II) ions having $t_{2g}^3e_g^2$ electronic configuration with *S*=5/2. This suggests dominant antiferromagnetic exchange in **1**, which is also evident from further decrease of the χT value on lowering the temperature down 60 K where χT reaches a value of 4.57 $cm^3mol^{-1}K$. Below this temperature, the χT *vs.* T plot shows a strong field dependence which is predicted for systems having large magnetic moment, exhibiting rapid saturation of magnetic moment at low temperatures. Upon further cooling, the χT value starts increasing smoothly till it reaches a maximum value of 49.72 $cm^3mol^{-1}K$ at 4.75 K, due to topology of AF exchange within 1D chains. After this, the χT value decreases to reach a final value of 26.29 $cm^3mol^{-1}K$ at 1.9 K indicating saturation of the magnetic moment at low temperatures. The Curie-Weiss fit for the magnetic moments also gives a θ_{CW} of -26 K which signifies the antiferromagnetic interactions present in the system (**Figure 5, right**).

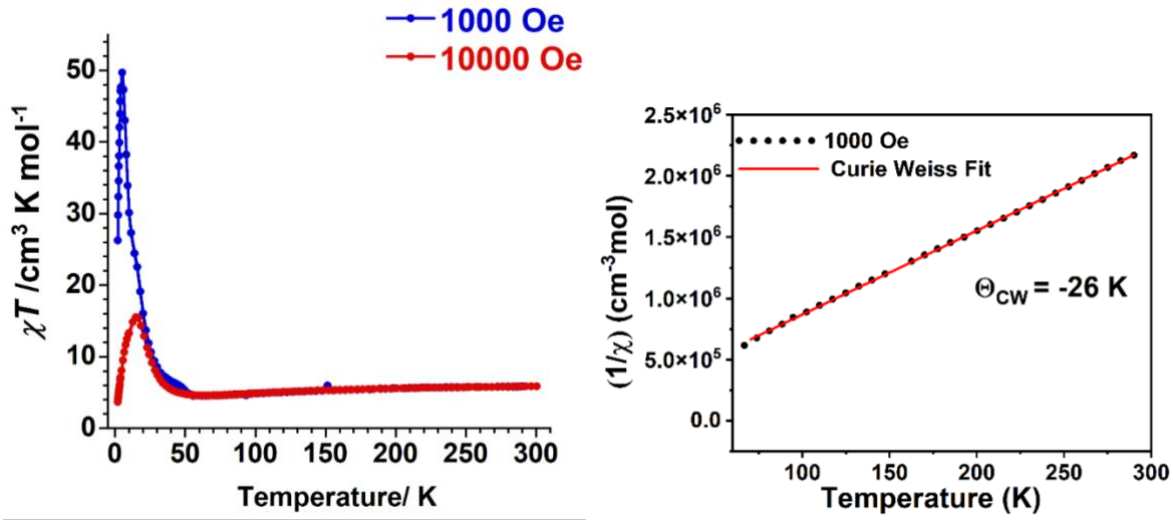

Figure 5: (Left): Temperature dependence of χT product for **1** at 1000 Oe (blue curve) and 10000 Oe (red curve) from 2-300 K. (Right): Curie-Weiss fit at 1000 Oe applied field.

Meanwhile, temperature dependent magnetic susceptibility curves of the desolvated phase **1.des** in the temperature range of 200 – 1.9 K at 1000 Oe applied DC field show the χT value of 5.65 $cm^3mol^{-1}K$ at 200 K which is lower than the spin-only χT value of 8.437 $cm^3mol^{-1}K$ (g= 2.0) that is expected for one $[CrMn_{1.5}]$ unit with Cr(III) ion having $t_{2g}^3e_g^0$ electronic configuration with S=3/2 and Mn(II) ions having $t_{2g}^3e_g^2$ electronic configuration with S=5/2 (**Figure 6**, right). This indicates the antiferromagnetic interactions of the two neighbouring metal centres. Upon lowering of temperature, the χT value decreases gradually to 5.05 $cm^3mol^{-1}K$ at 98 K below which it increases sharply to attain three maxima values of 55.09 $cm^3mol^{-1}K$ at 50 K, 55.90 $cm^3mol^{-1}K$ at 33 K and finally 73.4 $cm^3mol^{-1}K$ at 8.5 K, respectively below which the χT value falls rapidly to 21.61 $cm^3mol^{-1}K$ at 2 K. This behavior is indicative of ferrimagnetic ordering.

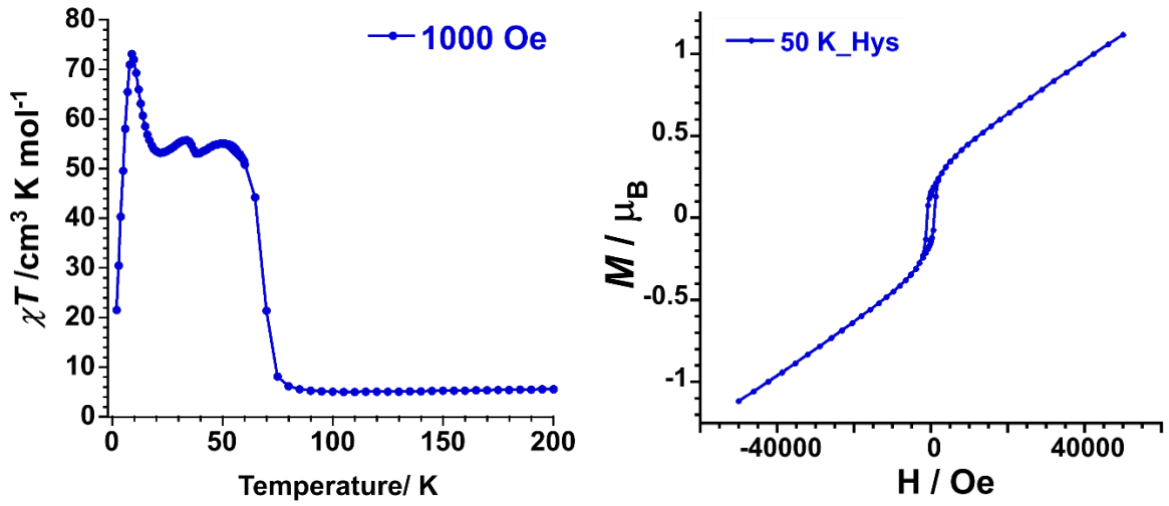

Figure 6: (Left): Temperature dependence of χT product for **1.des** at 1000 Oe (blue curve) from 2-200 K. (Right): Field dependence of the magnetization as M *vs.* H plots in hysteresis mode from -4 T to + 4T for **1.des** (right) at 50 K.

The field-dependent magnetization measurements for **1** from 0 – 5 T at 1.9, 4, 6 and 8 K (**Figure S13**, left) shows that the magnetization value is 3.65 μB at 1.9 K and 5 T. The value is much lower than the value expected for 1 Cr^{III}_{LS} (S = 3/2) and 1.5 Mn^{III}_{HS} (S = 5/2). M *vs.* H measurements were performed at 100 K to check for the presence of ferromagnetic impurities which were found to be absent (**Figure S14**, left). Also, the M *vs*. H/T curve (**Figure S13**, right) shows the non-superposition of data at different temperatures on a single master curve, indicating the presence of magnetic anisotropy in the system coming from the paramagnetic [$CrMn_{1.5}$] unit. The M *vs*. H measured in hysteresis mode from -5 T to +5 T (**Figure S14**, right) does not show the presence of any remnant magnetization. On the other hand, the magnetization value for the desolvated phase **1.des** is 3.5 μ_B at 2 K and 7 T. (less than 1 Cr^{III}_{LS} (S = 3/2) and 1.5 Mn^{III}_{HS} (S = 5/2)) (**Figure S15**, left), whereas the M *vs.* H in hysteresis mode does not show the presence of any opening of the curve at 2 K (**Figure S15**, right) but there is a small opening of the curve at 50 K with hysteresis width of 1851 Oe indicating remnant magnetization and soft behavior (**Figure 6**, right).

Ac susceptibility measurements of **1** show a clear maximum of the in-phase signal of the magnetic susceptibility (under zero DC field) as a function of temperature with different frequencies at temperature of 2.15 K (**Figure 7**). This indicates the presence of a ferrimagnetic ordering with T_C= 2.15 K. Also, a non-zero out-of-phase ac signal appears below 4 K (under zero DC field) and starts increasing with decrease of temperature reaching a maximum at 2.15 K (**Figure 7**). The peak maxima remain at this constant value under the application of different frequencies which indicates the absence of glassy behavior or superparamagnetism and shows a perfectly ordered state. Both the in-phase and out-of- phase magnetic susceptibility signals do not exhibit any field dependence against frequency (**Figure S16**) which shows the absence of slow relaxation of magnetization for this system. For the desolvated phase **1.des**,

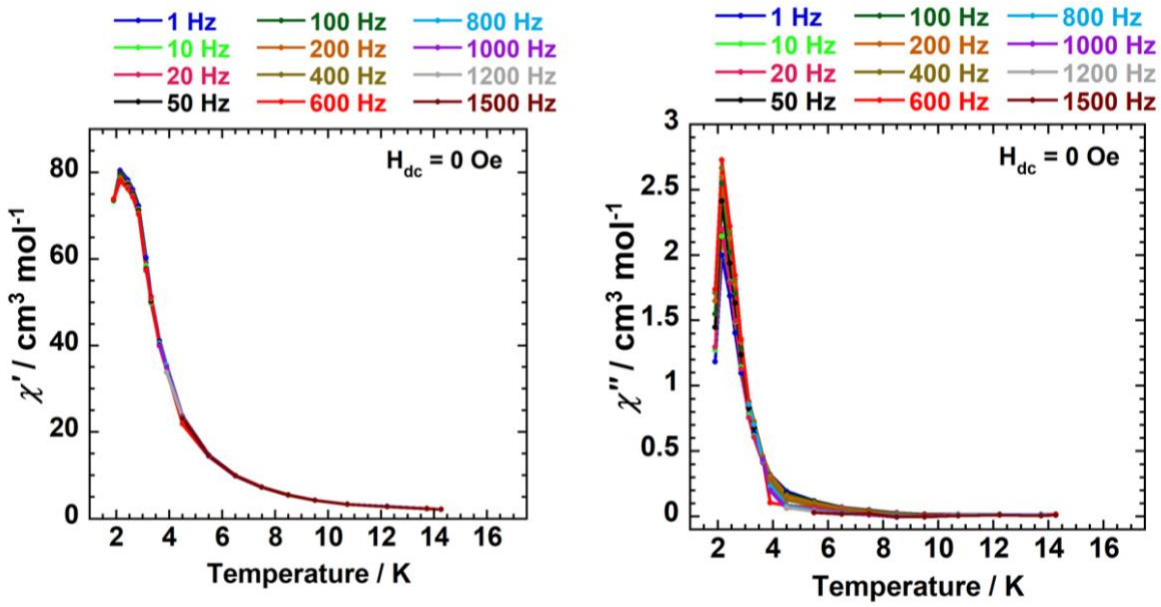

Figure 7: Temperature dependence of the in-phase (left) and out-of-phase (right) signal of magnetic susceptibility under zero dc field of **1** measured at different frequencies from 1-1500 Hz.

AC magnetic susceptibility curves at 0 Oe DC field show the in-phase and out-of-phase magnetic susceptibility with maxima at 9 K and 68 K, which does not shift with change of frequency, indicating a pure ordering (**Figure 8**, **Figure S17**). Also, for **1.des**, AC magnetic susceptibility curves at 1000 Oe DC field show the in-phase and out-of-phase magnetic susceptibility with maxima at 10 K which does not shift with change of frequency, indicating a pure ordering (**Figure 8**, **Figure S17**).

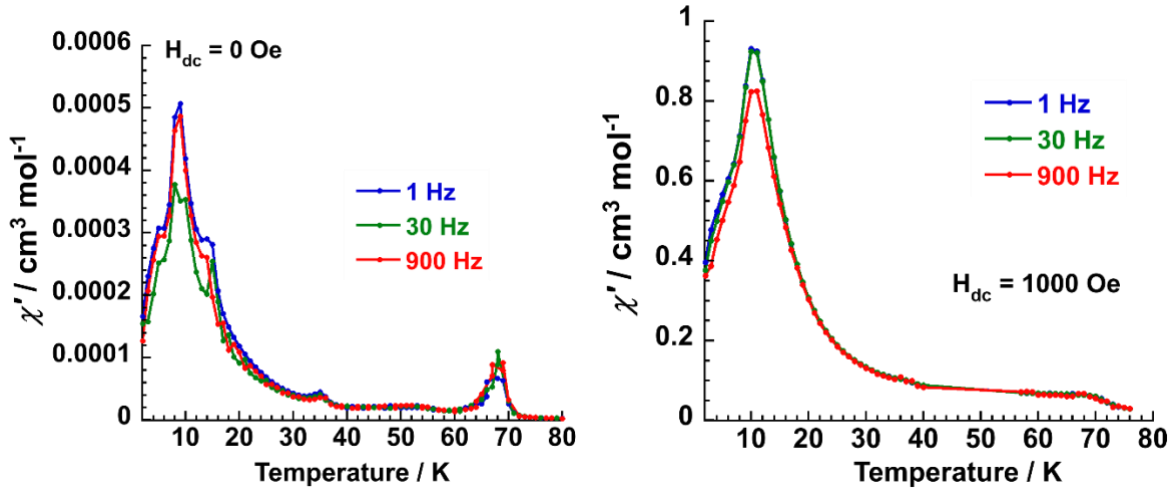

Figure 8: Temperature dependence of the in-phase signal of magnetic susceptibility under zero dc field (left) and 1000 Oe DC field (right) of **1.des** measured at different frequencies from 1-900 Hz.

Field cooled and zero-field cooled magnetization plots of **1** at 100 Oe (**Figure S18**) show the maximum χT value of 151.77 $cm^3mol^{-1}K$ and 156.14 $cm^3mol^{-1}K$ respectively at 2.89 K and does not bifurcate below this temperature. This also indicates the absence of glassy behavior or superparamagnetism. In case of the desolvated phase **1.des**, Field-Cooled (FC) and Zero Field-Cooled Magnetization measurements at 100 Oe show a bifurcation between the FC and ZFC curves below 66 K (blocking temperature T_B), indicating a glassy nature of the system (**Figure 9**).

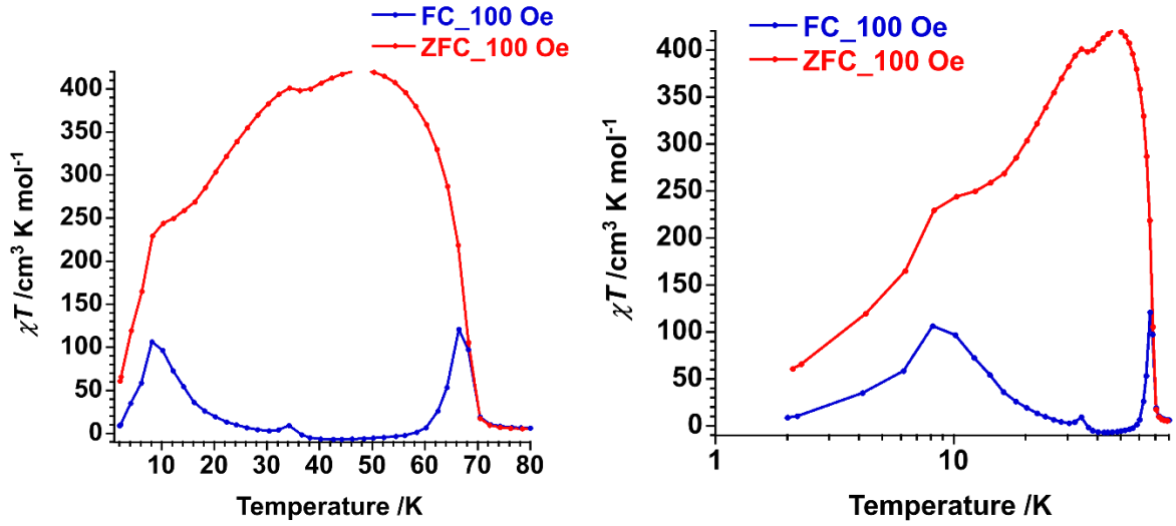

Figure 9: Field cooled and zero field cooled magnetization plots of **1.des** as a function of temperature at 100 Oe dc field (left) and in log scale (right).

Theoretical calculations and analysis of magnetic behavior

With the aim to better understand the magnetic behavior of **1**, the Density Functional Theory (DFT) was applied with the help of ORCA 5.0 computational package[24] to estimate the isotropic exchange among paramagnetic Mn^{II} and Cr^{III} ions. Herein, the proved hybrid functionals PBE0[25] was utilized and for selected dinuclear molecular motifs derived from the experimental structure, the high-spin (HS) and the broken-symmetry (BS) spin states were calculated. The energy difference of these two states, $\Delta = \varepsilon_{BS} - \varepsilon_{HS}$, helped to evaluate the exchange coupling among several Mn-Cr pairs. The isotropic exchange parameter J was calculated for spin Hamiltonian defined as $H = -J(S_1S_2)$ with the help of Ruiz[26] and Yamaguchi[27] formulas

$$J^{\text{Ruiz}} = 2\Delta / \left[\left(S_1 + S_2 \right) \left(S_1 + S_2 + 1 \right) \right] \quad (1)$$

$$J^{\text{Yam.}} = 2\Delta / \left[\left\langle S^2 \right\rangle_{\text{HS}} - \left\langle S^2 \right\rangle_{\text{BS}} \right] \quad (2)$$

Such calculations were done for four Mn-Cr dimers with different metal-metal distances as summarized in **Table 1**. The selected molecular structures with the calculated spin densities are depicted in **Figure S19**.

Table 1: The DFT calculated $<S^2>$ values, the energy difference between the BS and HS states, and the isotropic exchange parameters for Mn-Cr dimeric molecular fragments of **1**.

Pair	d(Mn-Cr) (Å)	$<S^2>_{HS}$	$<S^2>_{BS}$	Δ (cm^{-1})	J^{Ruiz} (cm^{-1})	J^{Yam} (cm^{-1})
Mn1-Cr1	5.399	20.1881	5.1893	-107.983	-10.8	-14.2
Mn1-Cr1	5.459	20.1883	5.1899	-98.780	-9.88	-13.2
Mn2-Cr1	5.416	20.0393	5.0376	-65.348	-6.53	-8.72
Mn2-Cr1	5.430	20.0390	5.0368	-82.627	-8.26	-11.0

Evidently, there is considerable antiferromagnetic exchange between all Mn^{II}-Cr^{III} couples, ranging from -7 to -11 cm^{-1} values when J^{Ruiz} is considered. As Mn^{II} ion and Cr^{III} ion have $t_{2g}^3e_g^2$ and $t_{2g}^3e_g^0$ electronic configurations, respectively, the metal-based magnetic orbitals based on three t_{2g} orbitals of these ions

facilitate significant orbital overlap through cyanide-bridging ligands resulting in dominant antiferromagnetic coupling[28].

Next, the attempt was made to utilize this information and model dc magnetic properties of **1** using spin Hamiltonian formalism. First, the model comprising one Mn_3Cr_2 unit was used as

$$\hat{H} = -J\left(\vec{S}_1^{Mn}\cdot\vec{S}_2^{Cr} + \vec{S}_2^{Cr}\cdot\vec{S}_3^{Mn} + \vec{S}_3^{Mn}\cdot\vec{S}_4^{Cr} + \vec{S}_4^{Cr}\cdot\vec{S}_5^{Mn}\right) + \mu_B\sum_i \vec{B}g\vec{S}_i \qquad (3)$$

for which temperature dependent χT product scaled per $[Mn_{1.5}Cr]$ unit was calculated as showed in **Figure 10**. Even this simplistic model nicely shows that with increasing antiferromagnetic exchange χT product (in cm^3Kmol^{-1}) at room temperature starts to decline from value 8.3 for J = -1 cm^{-1}, through value 7.5 for J = -10 cm^{-1} to value 6.7 for J = -20 cm^{-1} (**Figure 10**). This nicely explains much lower experimental value of χT product of **1** at room temperature. Second feature of the experimental magnetic data, the increase of χT product at lower temperatures, is also recovered successfully.

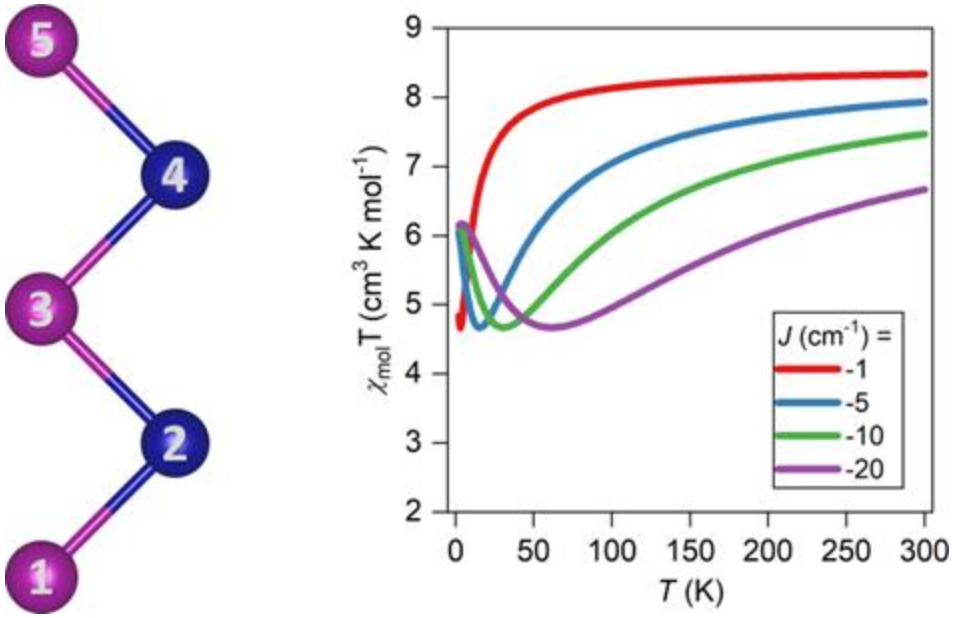

Figure 10: The scheme of spin Hamiltonian (Eq.3) with $S_1 = S_3 = S_5 = 5/2$ and $S_2 = S_4 = 3/2$ employed in calculation of temperature dependence of χT product (B = 0.1 T) of **1** for various J-values and g = 2.0. The magnetic data are scaled per $[Mn_{1.5}Cr]$ unit.

We are aware that model in Eq.3 is very simple and does not cover properly all magnetic interactions in the 2D sheets of **1**, thus more sophisticated spin Hamiltonian was proposed as

$$\hat{H} = -J\begin{pmatrix} \vec{S}_1^{\mathrm{Mn}} \cdot \vec{S}_2^{\mathrm{Cr}} + \vec{S}_1^{\mathrm{Mn}} \cdot \vec{S}_7^{\mathrm{Cr}} + \vec{S}_2^{\mathrm{Cr}} \cdot \vec{S}_3^{\mathrm{Mn}} + \vec{S}_2^{\mathrm{Cr}} \cdot \vec{S}_6^{\mathrm{Mn}} \\ + \vec{S}_2^{\mathrm{Cr}} \cdot \vec{S}_8^{\mathrm{Mn}} + \vec{S}_3^{\mathrm{Mn}} \cdot \vec{S}_4^{\mathrm{Cr}} + \vec{S}_3^{\mathrm{Mn}} \cdot \vec{S}_7^{\mathrm{Cr}} + \vec{S}_3^{\mathrm{Mn}} \cdot \vec{S}_9^{\mathrm{Cr}} \\ + \vec{S}_4^{\mathrm{Cr}} \cdot \vec{S}_5^{\mathrm{Mn}} + \vec{S}_4^{\mathrm{Cr}} \cdot \vec{S}_8^{\mathrm{Mn}} + \vec{S}_4^{\mathrm{Cr}} \cdot \vec{S}_{10}^{\mathrm{Mn}} + \vec{S}_5^{\mathrm{Mn}} \cdot \vec{S}_9^{\mathrm{Cr}} \\ + \vec{S}_6^{\mathrm{Mn}} \cdot \vec{S}_7^{\mathrm{Cr}} + \vec{S}_7^{\mathrm{Cr}} \cdot \vec{S}_8^{\mathrm{Mn}} + \vec{S}_8^{\mathrm{Mn}} \cdot \vec{S}_9^{\mathrm{Cr}} + \vec{S}_9^{\mathrm{Cr}} \cdot \vec{S}_{10}^{\mathrm{Mn}} \end{pmatrix} + \mu_{\mathrm{B}} \sum_i \vec{B} g \vec{S}_i \qquad (4)$$

in which two Mn_3Cr_2 units was incorporated as showed in **Figure 11**. However, increasing the number of spin centres from Mn_3Cr_2 to Mn_6Cr_4 led to enormous increase of spin states, namely, from $6^3 4^2 = 3\,456$ to $6^6 4^4 = 11\,943\,936$ spin states, which is not possible to analyse anymore. Therefore, we modified this model by lowering the spin values, namely spins 5/2 were replaced by spins 3/2, and spins 3/2 were replaced by spins 1/2, which led to 65 536 spin states. Such model is feasible to handle, and it should be able to qualitatively reproduce magnetic behaviour of **1**. Thus, the magnetic data were computed for series of *J*-values as depicted in **Figure 11.** The temperature profile of χT product is now more similar to experimental magnetic data, because there is larger increase of χT at lower temperatures below 100 K. Thus, it is evident that the interplay of antiferromagnetic exchange interactions in 1D ladder-like system indeed leads to the large increase of χT at lowest temperatures.

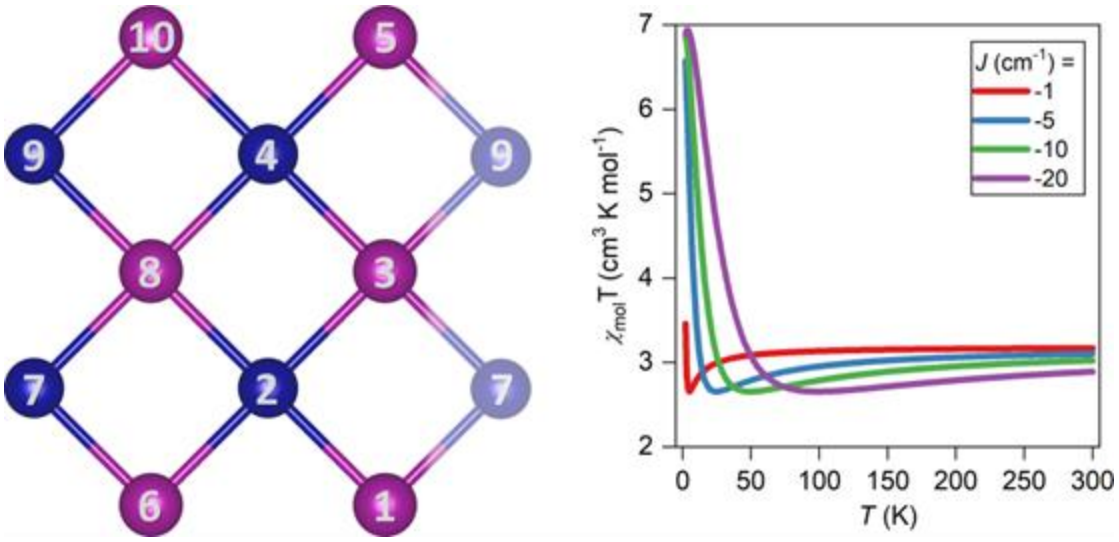

Figure 11: The scheme of spin Hamiltonian (Eq.4) with $S_A = S_1 = S_3 = S_5 = S_6 = S_8 = S_{10} = 3/2$ and $S_B = S_2 = S_4 = S_7 = S_9 = 1/2$ employed in calculation of temperature dependence of χT product (B = 0.1 T) of **1** for various J-values and g = 2.0. The magnetic data are scaled per $[(S_A)_{1.5}S_B]$ unit.

The last attempt to analyze magnetic behavior is based on the classical Monte-Carlo calculations with an open-source program EspinS.[29] Here, the general Hamiltonian comprising the magnetic exchange within the program is defined as

$$\hat{H} = -\frac{1}{2}\sum_{i,j} J_{ij}\left(\vec{S}_i \cdot \vec{S}_j\right) \qquad (5)$$

and the primitive cell was defined by Mn_9Cr_4 ions as showed in **Figure 12**. As this structural motif of **1** propagate in one crystal direction, the supercell was set as 1 x 10 x 1. The number of warm-up steps and Monte Carlo sampling steps were set to 500 000, and the magnetic susceptibility was calculated in 2-300 K temperature range with 2 K step. The results are depicted in **Figure 12** and the temperature profile of χT nicely reproduces the main features of experimental magnetic data of **1** and explains that despite antiferromagnetic exchange, the spin topology produces large magnetic moments of these 1D ladder-like chains.

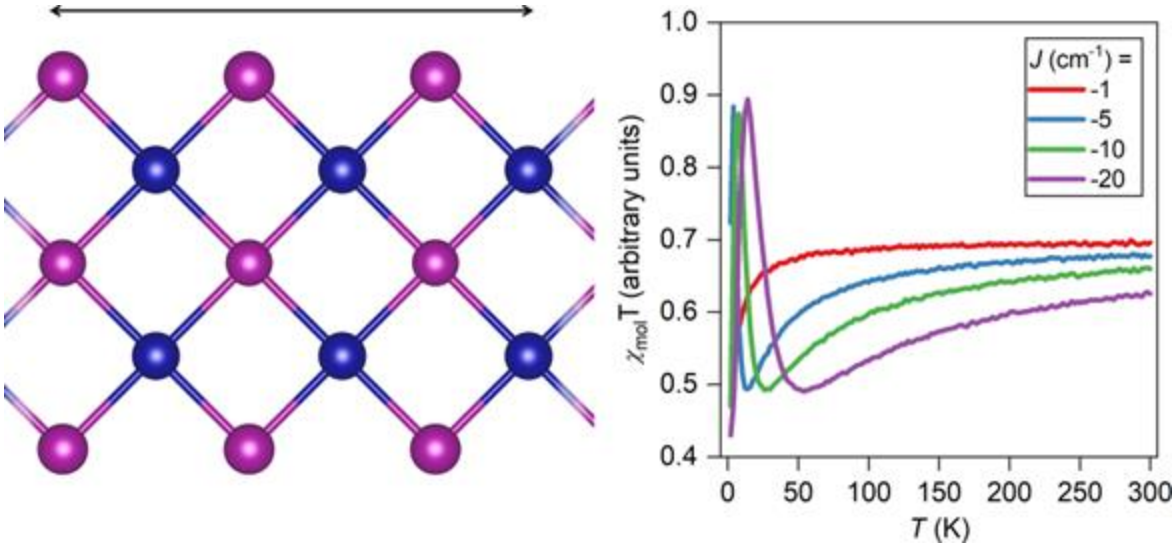

Figure 12: The scheme of primitive cell for classical Monte-Carlo calculations with ESpinS software and calculation of temperature dependence of χT product (arbitrary units) of **1** for various J-values with S_{Mn} = 5/2 (violet balls) and S_{Cr} = 3/2 (blue balls).

CONCLUSION

In conclusion, following the "building block" strategy using metallocyanate building block and monodentate ligand, we have successfully synthesized Cr^{III}-Mn^{II} two-dimensional network which on extension along b-axis forms a "stair" system. Detailed theoretical analysis revealed that considerable antiferromagnetic exchange among Mn(II) and Cr(III) ions mediated by cyanido ligands leads to large magnetic moments of 1D ladder-like units at lower temperatures due to topology of the exchange coupling. Moreover, these infinite ladder-like structures forms 2D stairs motif due to the hydrogen bonds and most likely these interactions result in strong ferrimagnetic long-range ordering at lowest temperatures. To understand the magnetic sponge property, the desolvated phase has also been synthesized which shows a significant change in the magnetic properties. We are currently analyzing the effect of magnetic sponge property on the ordering temperature.

EXPERIMENTAL SECTION

Detailed experimental procedures including materials and physical measurements, magnetic measurements and X-ray crystallography have been described in the supporting information.

*Synthesis of {[Mn(Me-im)$_3$(H$_2$O)][Cr(CN)$_6$][Mn(EtOH)$_2$]} (**1**)*

The reaction of $Mn(ClO_4)_2.6H_2O$ (6.3 mg, 0.025 mmol) with 1-Methylimidazole (8.2 mg, 0.1 mmol) in 8 mL of CH_3CN/EtOH (1:1) resulted in a colourless solution that was stirred for 15 min. This solution was added to a solution of $[NBu_4]_3[Cr(CN)_6]$ (23.3 mg, 0.025 mmol) in 8 mL of CH_3CN/EtOH (1:1) and stirred for 30 min. The resulting colourless solution was then filtered and kept for slow evaporation to obtain analytically pure single crystals of **1** in 32 % yield. Anal. Calcd. for $C_{20}H_{26}CrMn_{1.5}N_{12}O_2$ (M.W. 628.38 g mol^{-1}): C, 38.23; H, 4.17; Cr, 8.27; Mn, 17.49; N, 26.75; O, 5.09. Found: C, 38.18; H, 4.08; Cr, 8.24; Mn, 17.57; N, 26.81; O, 5.12. IR (KBr, cm^{-1}): 3637, 3297, 3135, 3098, 2962, 2930, 2145, 2130, 1629, 1537, 1518, 1474, 1444, 1424, 1372, 1337, 1283, 1246, 1233, 1109, 1088, 1029, 943, 897, 832, 761, 752, 662 and 616.

*Synthesis of **1.des***

To prepare the desolvated sample, single crystals of **1** were heated to 60 ºC under argon atmosphere for around 1 h which yielded colorless crystals of **1.des**. IR (ATR, cm^{-1}): 3140, 3125, 3102, 2962, 2930, 2876, 2151, 2123, 1616, 1538, 1518, 1473, 1422, 1372, 1285, 1250, 1233, 1108, 1084, 1027, 939, 892, 832, 778, 758, 745, 669, 658 and 617.

*Synthesis of **1.res***

To prepare the resolvated sample, the colorless crystals of **1.des** were subjected to slow diffusion of MeCN/EtOH (1:1) solution which gave colorless plate-like crystals of **1.res** after 2 d. IR (ATR, cm^{-1}): 3122, 3102, 2935, 2150, 2133, 1621, 1540, 1515, 1422, 1285, 1250, 1231, 1111, 1093, 1085, 1028, 945, 937, 892, 834, 825, 779, 763, 756, 745, 672, 659 and 618.

ASSOCIATED CONTENT

Supporting Information. Supporting Information is available free of charge on the ACS Publications website at DOI:

Experimental and spectral data, and crystallographic data (PDF).

Accession Codes. CCDC contains the supplementary crystallographic data for this paper. These data can be obtained free of charge via www.ccdc.cam.ac.uk/data_request/cif, or by emailing data_request@ccdc.cam.ac.uk, or by contacting The Cambridge Crystallographic Data Centre, 12 Union Road, Cambridge CB2 1EZ, UK; fax: +44 1223 336033.

AUTHOR INFORMATION

Corresponding Author

Radovan Herchel: *Email: radovan.herchel@upol.cz

Abhishake Mondal: *Email: *mondal@iisc.ac.in*

ORCID

Abhishake Mondal: 0000-0002-5061-2326

Mayurika Das: 0000-0002-2907-9854

Sujit Kamilya: 0000-0003-4881-0638

Sakshi Mehta: 0000-0002-1232-4489

Radovan Herchel: 0000-0001-8262-4666

Notes

The authors declare no competing financial interest.

ACKNOWLEDGEMENT

This research work is supported by the Indian Institute of Science (IISc), Bangalore, India the Department of Science and Technology, Mission on Nano Science and Technology (Nano Mission) (DST, Project No. DST/NM/TUE/QM-10/2019(G)/1), Government of India. M.D. and S.M. thank IISc and the Ministry of Education (MoE), and S.K. thanks the Council of Scientific & Industrial Research (CSIR) for the fellowship. R.H. acknowledges financial support from institutional sources of the Department of Inorganic Chemistry, Palacký University Olomouc, Czech Republic. R.H. is thankful to Prof. Mojtaba Alaei for discussion concerning the utilization of the ESpinS software.

REFERENCES

(1) Kahn, O. J. V. P., Inc., ,. Molecular magnetism. **1993**, 393. Miller, J. S.; Drillon, M. *Magnetism: Molecules to materials IV*; John Wiley & Sons, 2001.
(2) Leuenberger, M. N.; Loss, D. Quantum computing in molecular magnets. *Nature* **2001**, *410* (6830), 789-793. DOI: 10.1038/35071024.
(3) Bogani, L.; Wernsdorfer, W. Molecular spintronics using single-molecule magnets. *Nature Materials* **2008**, *7* (3), 179-186. DOI: 10.1038/nmat2133. Lehmann, J.; Gaita-Ariño, A.; Coronado, E.; Loss, D. Quantum computing with molecular spin systems. *Journal of Materials Chemistry* **2009**, *19* (12), 1672-1677, 10.1039/B810634G. DOI: 10.1039/B810634G. Camarero, J.; Coronado, E. Molecular vs. inorganic spintronics: the role of molecular materials and single molecules. *Journal of Materials Chemistry* **2009**, *19* (12), 1678-1684, 10.1039/B819594N. DOI: 10.1039/B819594N.
(4) Sessoli, R.; Gatteschi, D.; Caneschi, A.; Novak, M. A. Magnetic bistability in a metal-ion cluster. *Nature* **1993**, *365* (6442), 141-143. DOI: 10.1038/365141a0. Glaser, T.; Heidemeier, M.; Weyhermüller, T.; Hoffmann, R.-D.; Rupp, H.; Müller, P. Property-Oriented Rational Design of Single-Molecule Magnets: A C3-Symmetric Mn6Cr Complex based on Three Molecular Building Blocks with a Spin Ground State of St=21/2. **2006**, *45* (36), 6033-6037. DOI: https://doi.org/10.1002/anie.200600712. Miyasaka, H.; Takahashi, H.; Madanbashi, T.; Sugiura, K.-i.; Clérac, R.; Nojiri, H. Cyano-Bridged MnIII3MIII (MIII = Fe, Cr) Complexes: Synthesis, Structure, and Magnetic Properties. *Inorganic Chemistry* **2005**, *44* (17), 5969-5971. DOI: 10.1021/ic0505753. Ghosh, S.; Kamilya, S.; Das, M.; Mehta, S.; Boulon, M.-E.; Nemec, I.; Rouzières, M.; Herchel, R.; Mondal, A. Effect of Coordination Geometry on Magnetic Properties in a Series of Cobalt(II) Complexes and Structural Transformation in Mother Liquor. *Inorganic Chemistry* **2020**, *59* (10), 7067-7081. DOI: 10.1021/acs.inorgchem.0c00538. Boča, R.; Rajnák, C. Unexpected behavior of single ion magnets. *Coordination Chemistry Reviews* **2021**, *430*, 213657. DOI: https://doi.org/10.1016/j.ccr.2020.213657. Marin, R.; Brunet, G.; Murugesu, M. Shining New Light on Multifunctional Lanthanide Single-Molecule Magnets. *Angew Chem Int Ed Engl* **2021**, *60* (4), 1728-1746. DOI: 10.1002/anie.201910299 (acccessed 2020/04/12). Sørensen, M. A.; Hansen, U. B.; Perfetti, M.; Pedersen, K. S.; Bartolomé, E.; Simeoni, G. G.; Mutka, H.; Rols, S.; Jeong, M.; Zivkovic, I.; et al. Chemical tunnel-splitting-engineering in a dysprosium-based molecular nanomagnet. *Nature Communications* **2018**, *9* (1), 1292-1300. DOI: 10.1038/s41467-018-03706-x. Woodruff, D. N.; Winpenny, R. E. P.; Layfield, R. A. Lanthanide Single-Molecule Magnets. *Chemical Reviews* **2013**, *113* (7), 5110-5148. DOI: 10.1021/cr400018q.
(5) Clérac, R.; Miyasaka, H.; Yamashita, M.; Coulon, C. Evidence for Single-Chain Magnet Behavior in a MnIII−NiII Chain Designed with High Spin Magnetic Units: A Route to High Temperature Metastable Magnets. *Journal of the American Chemical Society* **2002**, *124* (43), 12837-12844. DOI: 10.1021/ja0203115. Miyasaka, H.; Nezu, T.; Sugimoto, K.; Sugiura, K.-i.; Yamashita, M.; Clérac, R. Linear NiII−MnIII2−NiII Tetramers: An Oligomeric Component of the MnIII2NiII Single-Chain Magnets. *Inorganic Chemistry* **2004**, *43* (18), 5486-5488. DOI: 10.1021/ic049457q. Coulon, C.; Clérac, R.; Wernsdorfer, W.; Colin, T.; Miyasaka, H. Realization of a Magnet Using an Antiferromagnetic Phase of Single-Chain Magnets. *Physical Review Letters* **2009**, *102* (16), 167204. DOI: 10.1103/PhysRevLett.102.167204. Ferbinteanu, M.; Miyasaka, H.; Wernsdorfer, W.; Nakata, K.; Sugiura, K.-i.; Yamashita, M.; Coulon, C.; Clérac, R. Single-Chain Magnet (NEt4)[Mn2(5-MeOsalen)2Fe(CN)6] Made of MnIII−FeIII−MnIII Trinuclear Single-Molecule Magnet with an ST = 9/2 Spin Ground State. *Journal of the American Chemical Society* **2005**, *127* (9), 3090-3099. DOI: 10.1021/ja0468123. Houard, F.; Evrard, Q.; Calvez, G.; Suffren, Y.; Daiguebonne, C.; Guillou, O.; Gendron, F.; Le Guennic, B.;

Guizouarn, T.; Dorcet, V.; et al. Chiral Supramolecular Nanotubes of Single-Chain Magnets. *Angewandte Chemie International Edition* **2020**, *59* (2), 780-784. DOI: 10.1002/anie.201913019 (acccessed 2020/04/12). Lutz, P.; Aguilà, D.; Mondal, A.; Pinkowicz, D.; Marx, R.; Neugebauer, P.; Fåk, B.; Ollivier, J.; Clérac, R.; van Slageren, J. Elementary excitations in single-chain magnets. *Physical Review B* **2017**, *96* (9), 094415-094420. DOI: 10.1103/PhysRevB.96.094415. Toma, L. M.; Delgado, F. S.; Ruiz-Pérez, C.; Carrasco, R.; Cano, J.; Lloret, F.; Julve, M. Synthesis, crystal structures and magnetic properties of single and double cyanide-bridged bimetallic Fe2IIICuII zigzag chains. *Dalton Transactions* **2004**, (18), 2836-2846, 10.1039/B407543A. DOI: 10.1039/B407543A.

(6) Coulon, C.; Miyasaka, H.; Clérac, R. Single-Chain Magnets:Theoretical Approach and Experimental Systems. In *Single-Molecule Magnets and Related Phenomena*, Winpenny, R. Ed.; Springer Berlin Heidelberg, 2006; pp 163-206. Christou, G.; Gatteschi, D.; Hendrickson, D. N.; Sessoli, R. Single-Molecule Magnets. *MRS Bulletin* **2000**, *25* (11), 66-71. DOI: 10.1557/mrs2000.226. Thomas, L.; Lionti, F.; Ballou, R.; Gatteschi, D.; Sessoli, R.; Barbara, B. Macroscopic quantum tunnelling of magnetization in a single crystal of nanomagnets. *Nature* **1996**, *383* (6596), 145-147. DOI: 10.1038/383145a0. Friedman, J. R.; Sarachik, M. P.; Tejada, J.; Ziolo, R. Macroscopic Measurement of Resonant Magnetization Tunneling in High-Spin Molecules. *Physical Review Letters* **1996**, *76* (20), 3830-3833. DOI: 10.1103/PhysRevLett.76.3830.

(7) Ferlay, S.; Mallah, T.; Ouahès, R.; Veillet, P.; Verdaguer, M. A room-temperature organometallic magnet based on Prussian blue. *Nature* **1995**, *378* (6558), 701-703. DOI: 10.1038/378701a0.

(8) Entley, W. R.; Girolami, G. S. High-Temperature Molecular Magnets Based on Cyanovanadate Building Blocks: Spontaneous Magnetization at 230 K. **1995**, *268* (5209), 397-400. DOI: 10.1126/science.268.5209.397 %J Science.

(9) Kahn, O.; Larionova, J.; Yakhmi, J. V. Molecular Magnetic Sponges. *Chemistry – A European Journal* **1999**, *5* (12), 3443-3449. DOI: https://doi.org/10.1002/(SICI)1521-3765(19991203)5:12<3443::AID-CHEM3443>3.0.CO;2-# (acccessed 2023/10/10).

(10) Beltran, L. M. C.; Long, J. R. Directed Assembly of Metal−Cyanide Cluster Magnets. *Accounts of Chemical Research* **2005**, *38* (4), 325-334. DOI: 10.1021/ar040158e.

(11) L. Heinrich, J.; A. Berseth, P.; R. Long, J. Molecular Prussian Blue analogues: synthesis and structure of cubic Cr4Co4(CN)12 and Co8(CN)12 clusters. *Chemical Communications* **1998**, (11), 1231-1232, 10.1039/A802351D. DOI: 10.1039/A802351D. Verdaguer, M.; Bleuzen, A.; Marvaud, V.; Vaissermann, J.; Seuleiman, M.; Desplanches, C.; Scuiller, A.; Train, C.; Garde, R.; Gelly, G. J. C. C. R. Molecules to build solids: high TC molecule-based magnets by design and recent revival of cyano complexes chemistry. **1999**, *190*, 1023-1047. Ohba, M.; Ōkawa, H. Synthesis and magnetism of multi-dimensional cyanide-bridged bimetallic assemblies. *Coordination Chemistry Reviews* **2000**, *198* (1), 313-328. DOI: https://doi.org/10.1016/S0010-8545(00)00233-2. Černák, J.; Orendáč, M.; Potočňák, I.; Chomič, J.; Orendáčová, A.; Skoršepa, J.; Feher, A. Cyanocomplexes with one-dimensional structures: preparations, crystal structures and magnetic properties. *Coordination Chemistry Reviews* **2002**, *224* (1), 51-66. DOI: https://doi.org/10.1016/S0010-8545(01)00375-7.

(12) Shatruk, M.; Avendano, C.; Dunbar, K. R. Cyanide-Bridged Complexes of Transition Metals: A Molecular Magnetism Perspective. In *Progress in Inorganic Chemistry*, 2009; pp 155-334. Weihe, H.; Güdel, H. U. Quantitative Interpretation of the Goodenough−Kanamori Rules: A Critical Analysis. *Inorganic Chemistry* **1997**, *36* (17), 3632-3639. DOI: 10.1021/ic961502+. Miller, J. S.; Manson, J. L. Designer magnets containing cyanides and nitriles. *Acc Chem Res* **2001**, *34* (7), 563-570. DOI: 10.1021/ar0000354 From NLM. Mondal, A.; Li, Y.; Seuleiman, M.; Julve, M.; Toupet, L.; Buron-Le

Cointe, M.; Lescouëzec, R. On/Off Photoswitching in a Cyanide-Bridged {Fe2Co2} Magnetic Molecular Square. *Journal of the American Chemical Society* **2013**, *135* (5), 1653-1656. DOI: 10.1021/ja3087467. Mondal, A.; Li, Y.; Herson, P.; Seuleiman, M.; Boillot, M.-L.; Rivière, E.; Julve, M.; Rechignat, L.; Bousseksou, A.; Lescouëzec, R. Photomagnetic effect in a cyanide-bridged mixed-valence {FeII2FeIII2} molecular square. *Chemical Communications* **2012**, *48* (45), 5653-5655, 10.1039/C2CC17835D. DOI: 10.1039/C2CC17835D. Kamilya, S.; Ghosh, S.; Li, Y.; Dechambenoit, P.; Rouzières, M.; Lescouëzec, R.; Mehta, S.; Mondal, A. Two-Step Thermoinduced Metal-to-Metal Electron Transfer and ON/OFF Photoswitching in a Molecular [Fe2Co2] Square Complex. *Inorganic Chemistry* **2020**, *59* (17), 11879-11888. DOI: 10.1021/acs.inorgchem.0c02053. Kaushik, K.; Ghosh, S.; Kamilya, S.; Rouzières, M.; Mehta, S.; Mondal, A. Reversible Photo- and Thermo-Induced Spin-State Switching in a Heterometallic {5d-3d} W2Fe2 Molecular Square Complex. *Inorganic Chemistry* **2021**, *60* (10), 7545-7552. DOI: 10.1021/acs.inorgchem.1c01014.

(13) Nowicka, B.; Heczko, M.; Rams, M.; Reczyński, M.; Gaweł, B.; Nitek, W.; Sieklucka, B. Solvatomagnetic Studies on Cyano-Bridged Bimetallic Chains Based on [Mn(cyclam)]3+ and Hexacyanometallates. *European Journal of Inorganic Chemistry* **2017**, *2017* (1), 99-106. DOI: https://doi.org/10.1002/ejic.201601007 (acccessed 2023/10/11). Yanai, N.; Kaneko, W.; Yoneda, K.; Ohba, M.; Kitagawa, S. Reversible Water-Induced Magnetic and Structural Conversion of a Flexible Microporous Ni(II)Fe(III) Ferromagnet. *Journal of the American Chemical Society* **2007**, *129* (12), 3496-3497. DOI: 10.1021/ja069166b. Pinkowicz, D.; Podgajny, R.; Bałanda, M.; Makarewicz, M.; Gaweł, B.; Łasocha, W.; Sieklucka, B. Magnetic Spongelike Behavior of 3D Ferrimagnetic {[MnII(imH)]2[NbIV(CN)8]}n with Tc = 62 K. *Inorganic Chemistry* **2008**, *47* (21), 9745-9747. DOI: 10.1021/ic801248f. Pinkowicz, D.; Podgajny, R.; Gaweł, B.; Nitek, W.; Łasocha, W.; Oszajca, M.; Czapla, M.; Makarewicz, M.; Bałanda, M.; Sieklucka, B. Double Switching of a Magnetic Coordination Framework through Intraskeletal Molecular Rearrangement. *Angewandte Chemie International Edition* **2011**, *50* (17), 3973-3977. DOI: https://doi.org/10.1002/anie.201100880 (acccessed 2024/01/19).

(14) Dehnicke, K. Book Review: The Chemistry of Cyano Complexes of the Transition of Metals. Organometallic Chemistry—A Series of Monographs. By A. G. Sharpe. **1976**, *15* (11), 709-709. DOI: https://doi.org/10.1002/anie.197607092. Nelson, K. J.; Giles, I. D.; Troff, S. A.; Arif, A. M.; Miller, J. S. Solvent-Enhanced Magnetic Ordering Temperature for Mixed-Valent Chromium Hexacyanovanadate(II), CrII0.5CrIII[VII(CN)6]·zMeCN, Magnetic Materials. *Inorganic Chemistry* **2006**, *45* (22), 8922-8929. DOI: 10.1021/ic0608896. Berlinguette, C. P.; Dragulescu-Andrasi, A.; Sieber, A.; Galán-Mascarós, J. R.; Güdel, H.-U.; Achim, C.; Dunbar, K. R. A Charge-Transfer-Induced Spin Transition in the Discrete Cyanide-Bridged Complex {[Co(tmphen)2]3[Fe(CN)6]2}. *Journal of the American Chemical Society* **2004**, *126* (20), 6222-6223. DOI: 10.1021/ja039451k. Berlinguette, C. P.; Dragulescu-Andrasi, A.; Sieber, A.; Güdel, H.-U.; Achim, C.; Dunbar, K. R. A Charge-Transfer-Induced Spin Transition in a Discrete Complex: The Role of Extrinsic Factors in Stabilizing Three Electronic Isomeric Forms of a Cyanide-Bridged Co/Fe Cluster. *Journal of the American Chemical Society* **2005**, *127* (18), 6766-6779. DOI: 10.1021/ja043162u. Shen, X.; Li, B.; Zou, J.; Hu, H.; Xu, Z. The first cyano-bridged heptanuclear Mn(III)6Fe(III) cluster: crystal structure and magnetic properties of [{Mn(salen)·H2O}6Fe(CN)6][Fe(CN)6]·6H2O. *Journal of Molecular Structure* **2003**, *657* (1), 325-331. DOI: https://doi.org/10.1016/S0022-2860(03)00452-6. Li, S.; Xiong, J.; Yuan, Q.; Zhu, W.-H.; Gong, H.-W.; Wang, F.; Feng, C.-Q.; Wang, S.-Q.; Sun, H.-L.; Gao, S. Effect of the Transition Metal Ions on the Single-Molecule Magnet Properties in a Family of Air-Stable 3d–4f Ion-Pair Compounds with Pentagonal

Bipyramidal Ln(III) Ions. *Inorganic Chemistry* **2021**, *60* (24), 18990-19000. DOI: 10.1021/acs.inorgchem.1c02828.
(15) Dreiser, J.; Schnegg, A.; Holldack, K.; Pedersen, K. S.; Schau-Magnussen, M.; Nehrkorn, J.; Tregenna-Piggott, P.; Mutka, H.; Weihe, H.; Bendix, J.; et al. Frequency-Domain Fourier-Transform Terahertz Spectroscopy of the Single-Molecule Magnet (NEt4)[Mn2(5-Brsalen)2(MeOH)2Cr(CN)6]. **2011**, *17* (27), 7492-7498. DOI: https://doi.org/10.1002/chem.201100581. Zhang, D.; Wang, H.; Chen, Y.; Ni, Z.-H.; Tian, L.; Jiang, J. Hydrogen-Bond Directed Cyanide-Bridged Molecular Magnets Derived from Polycyanidemetalates and Schiff Base Manganese(III) Compounds: Synthesis, Structures, and Magnetic Properties. *Inorganic Chemistry* **2009**, *48* (23), 11215-11225. DOI: 10.1021/ic901530p. Zhou, H.-B.; Wang, J.; Wang, H.-S.; Xu, Y.-L.; Song, X.-J.; Song, Y.; You, X.-Z. Synthesis, Structure, and Magnetic Properties of Three 1D Chain Complexes Based on High-Spin Metal–Cyanide Clusters: [MnIII6MIII] (M = Cr, Fe, Co). *Inorganic Chemistry* **2011**, *50* (15), 6868-6877. DOI: 10.1021/ic102527h. Mallah, T.; Thiébaut, S.; Verdaguer, M.; Veillet, P. High-Tc Molecular-Based Magnets: Ferrimagnetic Mixed-Valence Chromium(III)-Chromium(II) Cyanides with Tc at 240 and 190 Kelvin. *Science (New York, N.Y.)* **1993**, *262* (5139), 1554-1557. DOI: 10.1126/science.262.5139.1554 From NLM. Holmes, S. M.; Girolami, G. S. Sol−Gel Synthesis of KVII[CrIII(CN)6]·2H2O: A Crystalline Molecule-Based Magnet with a Magnetic Ordering Temperature above 100 °C. *Journal of the American Chemical Society* **1999**, *121* (23), 5593-5594. DOI: 10.1021/ja990946c. Ohba, M.; Usuki, N.; Fukita, N.; Ōkawa, H. [Mn(en)](3) [Cr(CN)(6)](2) ·4 H(2) O: A Three-Dimensional Dimetallic Ferrimagnet (T(c) =69 K) with a Defective Cubane Unit. *Angewandte Chemie (International ed. in English)* **1999**, *38* (12), 1795-1798. DOI: 10.1002/(sici)1521-3773(19990614)38:12<1795::Aid-anie1795>3.0.Co;2-i From NLM. Kou, H. Z.; Gao, S.; Zhang, J.; Wen, G. H.; Su, G.; Zheng, R. K.; Zhang, X. X. Unexpected assembly of a unique cyano-bridged three-dimensional Cu3Cr2 ferromagnet. *J Am Chem Soc* **2001**, *123* (47), 11809-11810. DOI: 10.1021/ja016656p From NLM.
(16) Shen, X.; Zhang, Q.; Zhou, H.; Zhou, H.; Yuan, A. Syntheses, crystal structures and magnetic properties of two low-dimensional cyano-bridged CrIII–MnII/III assemblies. *New Journal of Chemistry* **2012**, *36* (5), 1180-1186, 10.1039/C2NJ20966G. DOI: 10.1039/C2NJ20966G. Alexandru, M.-G.; Visinescu, D.; Shova, S.; Andruh, M.; Lloret, F.; Cano, J.; Julve, M. Three different types of bridging ligands in a 3d–3d′–3d″ heterotrimetallic chain. *Dalton Transactions* **2018**, *47* (4), 1010-1013, 10.1039/C7DT04586G. DOI: 10.1039/C7DT04586G.
(17) Casanova, D.; Llunell, M.; Alemany, P.; Alvarez, S. The Rich Stereochemistry of Eight-Vertex Polyhedra: A Continuous Shape Measures Study. *Chemistry – A European Journal* **2005**, *11* (5), 1479-1494. DOI: 10.1002/chem.200400799 (acccessed 2020/04/18).
(18) Ketkaew, R.; Tantirungrotechai, Y.; Harding, P.; Chastanet, G.; Guionneau, P.; Marchivie, M.; Harding, D. J. OctaDist: a tool for calculating distortion parameters in spin crossover and coordination complexes. *Dalton Transactions* **2021**, *50* (3), 1086-1096, 10.1039/D0DT03988H. DOI: 10.1039/D0DT03988H.
(19) Liu, X.; Roubeau, O.; Clérac, R. Cyanido-bridged bimetallic two-dimensional network based on dinuclear manganese(III) Schiff base complex and hexacyanochromate(III) building block. *Comptes Rendus Chimie* **2008**, *11* (10), 1182-1191. DOI: 10.1016/j.crci.2008.04.013. Yang, C.; Wang, Q. L.; Qi, J.; Ma, Y.; Yan, S. P.; Yang, G. M.; Cheng, P.; Liao, D. Z. Two novel cyanide-bridged bimetallic magnetic chains derived from manganese(III) Schiff bases and hexacyanochromate(III) building blocks. *Inorg Chem* **2011**, *50* (9), 4006-4015. DOI: 10.1021/ic102495t.

(20) Alexandru, M. G.; Visinescu, D.; Shova, S.; Andruh, M.; Lloret, F.; Cano, J.; Julve, M. Three different types of bridging ligands in a 3d-3d'-3d" heterotrimetallic chain. *Dalton Trans* **2018**, *47* (4), 1010-1013. DOI: 10.1039/c7dt04586g. Marvaud, V.; Decroix, C.; Scuiller, A.; Guyard-Duhayon, C.; Vaissermann, J.; Gonnet, F.; Verdaguer, M. Hexacyanometalate Molecular Chemistry: Heptanuclear Heterobimetallic Complexes; Control of the Ground Spin State. *Chemistry – A European Journal* **2003**, *9* (8), 1677-1691, https://doi.org/10.1002/chem.200390192. DOI: https://doi.org/10.1002/chem.200390192 (acccessed 2021/05/21).
(21) Atanasov, M.; Busche, C.; Comba, P.; El Hallak, F.; Martin, B.; Rajaraman, G.; van Slageren, J.; Wadepohl, H. Trinuclear {M1}CN{M2}2 Complexes (M1 = CrIII, FeIII, CoIII; M2 = CuII, NiII, MnII). Are Single Molecule Magnets Predictable? *Inorganic Chemistry* **2008**, *47* (18), 8112-8125. DOI: 10.1021/ic800556c. Zhu, M.; Liu, J.; Su, J.; Meng, B.; Feng, Y.; Jia, B.; Peng, T.; Qi, Z.; Gao, E. Two MnII, CuII complexes derived from 3,5-bis(1-imidazoly) pyridine: Synthesis, DNA binding, Molecular docking and cytotoxicity studies. *Applied Organometallic Chemistry* **2019**, *33* (1), e4676, https://doi.org/10.1002/aoc.4676. DOI: https://doi.org/10.1002/aoc.4676 (acccessed 2021/05/21).
(22) Alexander, J. J.; Gray, H. B. Electronic structures of hexacyanometalate complexes. *Journal of the American Chemical Society* **1968**, *90* (16), 4260-4271. DOI: 10.1021/ja01018a013.
(23) Hoeke, V.; Heidemeier, M.; Krickemeyer, E.; Stammler, A.; Bogge, H.; Schnack, J.; Postnikov, A.; Glaser, T. Environmental influence on the single-molecule magnet behavior of [Mn(III)6Cr(III)]3+: molecular symmetry versus solid-state effects. *Inorg Chem* **2012**, *51* (20), 10929-10954. DOI: 10.1021/ic301406j. Shatruk, M.; Chambers, K. E.; Prosvirin, A. V.; Dunbar, K. R. Systematic Investigation of Trigonal-Bipyramidal Cyanide-Bridged Clusters of the First-Row Transition Metals. *Inorganic Chemistry* **2007**, *46* (13), 5155-5165. DOI: 10.1021/ic061856t.
(24) Neese, F. Software update: The ORCA program system—Version 5.0. *WIREs Computational Molecular Science* **2022**, *12* (5), e1606, https://doi.org/10.1002/wcms.1606. DOI: https://doi.org/10.1002/wcms.1606 (acccessed 2023/05/01).
(25) Adamo, C.; Barone, V. Toward reliable density functional methods without adjustable parameters: The PBE0 model. *The Journal of Chemical Physics* **1999**, *110* (13), 6158-6170. DOI: 10.1063/1.478522 (acccessed 5/1/2023).
(26) Ruiz, E.; Cano, J.; Alvarez, S.; Alemany, P. Broken symmetry approach to calculation of exchange coupling constants for homobinuclear and heterobinuclear transition metal complexes. *Journal of Computational Chemistry* **1999**, *20* (13), 1391-1400, https://doi.org/10.1002/(SICI)1096-987X(199910)20:13<1391::AID-JCC6>3.0.CO;2-J. DOI: https://doi.org/10.1002/(SICI)1096-987X(199910)20:13<1391::AID-JCC6>3.0.CO;2-J (acccessed 2023/05/01).
(27) Soda, T.; Kitagawa, Y.; Onishi, T.; Takano, Y.; Shigeta, Y.; Nagao, H.; Yoshioka, Y.; Yamaguchi, K. Ab initio computations of effective exchange integrals for H-H, H-He-H and Mn ₂O ₂ complex: comparison of broken-symmetry approaches. *Chemical Physics Letters* **2000**, *319*, 223-230. DOI: 10.1016/S0009-2614(00)00166-4.
(28) Verdaguer, M.; Girolami, G. S. Magnetic Prussian Blue Analogs. In *Magnetism: Molecules to Materials V*, 2004; pp 283-346.
(29) Rezaei, N.; Alaei, M.; Akbarzadeh, H. ESpinS: A program for classical Monte-Carlo simulations of spin systems. *Computational Materials Science* **2022**, *202*, 110947. DOI: https://doi.org/10.1016/j.commatsci.2021.110947.

For Table of Contents Only

A one-dimensional ladder-chain network of heterobimetallic Cr^{III}-Mn^{II} "stair" system has been synthesized which undergoes sponge behavior and exhibits ferrimagnetic ordering at low temperature, that upon desolvation shows a marked difference in the magnetic properties.